Magnetically textured y-Fe2O3 nanoparticles in a silica gel matrix: structural and magnetic properties

Florian Bentivegna, J. Ferre, M. Nyvlt, J.P. Jamet, Dominique Imhoff, Michael Canva, Alain Brun, P. Veillet, Š Višňovský, Frédéric Chaput, et al.

HAL Id: hal-00668322

https://hal-iogs.archives-ouvertes.fr/hal-00668322

Submitted on 9 Feb 2012

Magnetically textured γ-Fe$_2$O$_3$ nanoparticles in a silica gel matrix: Structural and magnetic properties

F. Bentivegna[a)]
Institut d'Optique Théorique et Appliquée, URA CNRS 14, Bat 503, Université Paris XI, 91405 Orsay, France

J. Ferré[b)]
Laboratoire de Physique des Solides, URA CNRS 2, Bat 510, Université Paris XI, 91405 Orsay, France

M. Nývlt
Institute of Physics, Charles University, Ke Karlovu 5, 12116 Praha 2, Czech Republic

J. P. Jamet and D. Imhoff
Laboratoire de Physique des Solides, URA CNRS 2, Bat 510, Université Paris XI, 91405 Orsay, France

M. Canva and A. Brun
Institut d'Optique Théorique et Appliquée, URA CNRS 14, Bat 510, Université Paris XI, 91405 Orsay, France

P. Veillet
Institut d'Electronique Fondamentale, URA CNRS 22, Bat 220 Université Paris XI, 91405 Orsay, France

Š. Višňovský
Institute of Physics, Charles University, Ke Karlovu 5, 12116 Praha 2, Czech Republic

F. Chaput and J. P. Boilot
Laboratoire de Physique de la Matière Condensée, URA CNRS 1254, 91128 Palaiseau Cedex, France

This paper is devoted to magnetic and structural properties of anisotropic γ-Fe$_2$O$_3$ superparamagnetic particles dispersed in a transparent xerogel matrix. The effect of frozen anisotropy axes and magnetic texture, induced by a magnetic field applied during the solidification of the matrix on the in-field magnetization process, is studied by alternating gradient force magnetometry and first and second order magneto-optical effects. The changes of magnetization curves with respect to the ferrofluid solution at the same particle concentration are interpreted on the basis of an existing statistical approach extended to systems with particle size distribution, which has to be taken into account for real samples. A very good agreement between the experiment and theory was achieved for a log-normal distribution of diameters which well resembles that deduced from electron microscopy observations in different imaging modes. This structural analysis states the parameter values used in calculations and confirms the relevance of basic assumptions of the model for the specimens studied. The experimental results and the related theoretical discussion should be of use to understand magnetic properties of other magnetically textured superparamagnetic systems. © *1998 American Institute of Physics.* [S0021-8979(98)00412-5]

I. INTRODUCTION

Nanophase materials composed of small nanometric-sized magnetic particles are the subject of intense current research since they exhibit novel electronic, magnetic and optical properties. It is now possible to design and synthesize materials containing dispersed superparamagnetic particles with reasonably well calibrated shape and size. Up to now only a few experimental works were devoted to small ferrofluid particles embedded in polymer or glass matrices.[1–6] Although the possibility of freezing the positions of particles is

very promising, up to now there has been practically no experimental study of the interesting case of magnetically oriented particles in solid matrices, also called *magnetically textured media*.[7,8] Such a system is prepared starting from a polymeric or sol–ferrofluid solution, which is solidified as a gel under magnetic field.[9] From the theoretical side the low field susceptibility[8,10] and the field induced magnetization curves[7] have been examined in such magnetically textured systems. Large permanent linear birefringence has also been recently evidenced in textured γ-Fe$_2$O$_3$ maghemite particles embedded in a hard and highly transparent gel matrix.[3] This gives direct proof that oriented magnetic particles are locked in the gel matrix.

This study is focused on gels elaborated from highly diluted ferrofluid solutions for which we can neglect the magnetic interaction between particles. This also supports

the effect of the surfactant to avoid the aggregation of magnetic particles or the possible formation of chains of particles which could be stabilized during the gel preparation under magnetic field in the case of a large concentration of particles.[11,12] From a magnetic point of view and according to Néel's theory,[13] small-size particles with diameters D smaller than 15 nm are single domain at low temperatures. At room temperature and when $\eta = KV/kT < 25$ (K being the anisotropy constant, V the volume of the particle), these single particles exhibit a superparamagnetic behavior.[14]

In this paper we report on magnetic properties of γ-Fe$_2$O$_3$ maghemite superparamagnetic particles dispersed in a gel matrix. The magnetism of this medium is studied after inducing a magnetic texture by a field $\boldsymbol{B}_p$ applied during the solidification of the matrix. The consequences of this induced anisotropy on the in-field magnetization and related magneto-optical effects at first order (Faraday rotation and magnetic circular dichroism) and second order (magnetic linear dichroism and birefringence) in magnetization are discussed. The results are compared with a reference ferrofluid solution having the same volume fraction of particles as the gel samples.

The differences between the normalized magnetization curves for magnetically textured samples and ferrofluids were previously calculated by Raikher[7] in the frame of a statistical approach for an assembly of monodispersed (having the same size) particles.

In Sec. II we will extend Raikher's model to polydisperse systems having a distribution of particle diameters. In Sec. III we shall recall the preparation method and report on structural properties of the samples, experimental techniques employed in this study, as well as the treatment of the experimental data. A direct comparison between magnetic measurements by magnetometry and magneto-optics in the different samples will be reported in Sec. IV. We shall stress there the influence of the magnetic texture on the anisotropy of magnetization.

II. THEORETICAL ASPECTS AND BASIC FORMULAS

A. Magnetization of a monodispersed superparamagnetic system

Let us start from a single domain particle[7] having a magnetic moment μ, oriented in the $\boldsymbol{m}$ direction and with the uniaxial anisotropy axis oriented along $\boldsymbol{n}$. In an external magnetic field with induction of magnitude B and direction $\boldsymbol{b}$ the energy of the particle is expressed as

$$E = -\mu B(\boldsymbol{m}\cdot\boldsymbol{b}) - KV(\boldsymbol{m}\cdot\boldsymbol{n})^2, \tag{1}$$

$\boldsymbol{m}$, $\boldsymbol{n}$ and $\boldsymbol{b}$ being unit vectors. The first term in expression (1) represents the potential (or Zeeman) energy of the magnetic dipole in the magnetic field, while the second one stands for the anisotropy energy. The contribution of the shape anisotropy is considered here to be negligible, although in our specimens some particles exhibit a small ellipticity, as we shall see later. In the ferrofluid thermal fluctuations cause a random Brownian rotation of the particles. Physical properties of the system depend on the ratio be-

tween the magnetic [expression (1)] and the thermal (kT) energies. Therefore in the following expressions we will introduce the dimensionless parameters

$$\xi = \frac{\mu B}{kT} \quad \text{and} \quad \eta = \frac{KV}{kT}. \tag{2}$$

An assembly of identical particles submitted to an external magnetic field exhibits a magnetization M along $\boldsymbol{b}$, so that

$$\frac{M}{M_s} = \frac{\partial}{\partial\xi} \ln Z, \tag{3}$$

where M_s is the saturated magnetization and Z the partition function.

For the particles, which can freely rotate in the ferrofluid under field, the partition function is written,

$$Z(\xi,\eta) = \int\int \exp[\xi(\boldsymbol{m}\cdot\boldsymbol{b}) + \eta(\boldsymbol{m}\cdot\boldsymbol{n})^2]d\boldsymbol{n}\,d\boldsymbol{m}, \tag{4}$$

where integration runs over all directions $\boldsymbol{n}$ and $\boldsymbol{m}$ such as

$$Z(\xi,\eta) = 16\pi^2\,\frac{\sinh\xi}{\xi}\int_0^1 \exp(\eta y^2)dy. \tag{5}$$

$Z(\xi,\eta)$ can thus be written as a product of two terms which are related to Zeeman and anisotropy energies. In other words, the magnetization does not depend on the anisotropy because of the rotational freedom of particles in the solution. Then the magnetization of the ferrofluid, M_f, related to the degree of alignment of the magnetic moments of the particles, depends only on the ratio ξ between Zeeman and thermal energies

$$\frac{M_f}{M_s} = \frac{\partial}{\partial\xi} \ln\left(\frac{\sinh\xi}{\xi}\right) = L(\xi), \tag{6}$$

where $L(\xi)$ is the usual Langevin function

$$L(\xi) = \coth\xi - \xi^{-1}. \tag{7}$$

The magnetization process is consequently not influenced by the anisotropy of the particles, provided that the particle easy axis directions $\boldsymbol{n}$ are distributed at thermal equilibrium.[10]

During the solidification of the matrix the orientations of the particles become fixed[15,16] according to the statistic distribution of the anisotropy axes at preparation temperature. For such a frozen system the in-field magnetization process then takes place through the Néel rotation of the magnetic moments away from the easy axis particle directions, which are not aligned along the applied field. The magnetic properties at temperatures $T > 0$ K are then, of course, dependent on the orientation of the frozen easy axes of the particles relatively to the applied field, i.e., on the anisotropy.

In order to obtain the in-field magnetization curve of an assembly of superparamagnetic particles with frozen anisotropy axes let us start from the partition function of the particles having a fixed anisotropy axis $\boldsymbol{n}$[7]

$$Z(\xi,\eta,\boldsymbol{b},\boldsymbol{n}) = \int \exp[\xi(\boldsymbol{m}\cdot\boldsymbol{b}) + \eta(\boldsymbol{m}\cdot\boldsymbol{n})^2]d\boldsymbol{m}. \tag{8}$$

Now, if a preparation field B_p is applied during the solidification of the matrix, the particles tend to orient themselves along b, generating a magnetic texture. Using Eqs. (4) and (8), and replacing ξ by ξ_p and b by b_p to indicate that these quantities are related to the preparation process, the distribution of the particle easy anisotropy axes n can be described by the density

$$f(\xi_p, \eta, b_p, n) = \frac{Z(\xi_p, \eta, b_p, n)}{Z(\xi_p, \eta)}. \tag{9}$$

The magnetization curve results from the contributions of all particles

$$\frac{M(b, b_p, \xi, \xi_p, \eta)}{M_s} = \frac{\partial}{\partial \xi} \int f(\xi_p, \eta, b_p, n)$$
$$\times \ln Z(\xi, \eta, b, n) dn. \tag{10}$$

A convenient way to evaluate the effect of frozen anisotropy axes on the in-field magnetization curve is to plot the difference[7]

$$\delta M_p = \frac{M_p}{M_s} - L(\xi), \tag{11}$$

where the subscript p deals with the sample preparation process.

B. Uniform distribution of easy anisotropy axes

If the gel is synthesized in the absence of magnetic field, the easy anisotropy axes are uniformly distributed in all directions. Then the density of probability [Eq. (9)] becomes $f = (4\pi)^{-1}$ and the associated magnetization M_0 is expressed as

$$\frac{M_0}{M_s} = \frac{1}{4\pi} \frac{\partial}{\partial \xi} \int \ln Z(\xi, \eta, b, n) dn. \tag{12}$$

This case was previously studied by Yasumori *et al.*,[10] who deduced an analytical expression for the ratio M_0/M_s, which they compared to the Langevin function $L(\xi)$. They also proved that the initial (or low field) susceptibility is the same as for $L(\xi)$, being equal to $\xi/3$ independently of η, as also found by Chantrell *et al.*[8]

The effect of a fixed uniform distribution of easy anisotropy axes on the magnetization process is shown in Fig. 1, on the plot of δM_0 [expression (11)] for different values of η, demonstrating the important role of the anisotropy constant K. It is obviously more difficult to magnetize such a sample than the corresponding ferrofluid solution for which the magnetization curve is described by $L(\xi)$. So, as expected, this ''resistance to a magnetization'' increases with η, i.e., with the anisotropy constant K. The difference δM_0 becomes very small when the anisotropy energy of each particle is negligible with respect to its Zeeman energy,[5] i.e., when $\eta \ll \xi$. For a given η, the absolute value of the difference δM_0 exhibits a peak at a given value of ξ. For larger values of the parameter η this peak slightly shifts towards higher ξ values. Figure 1 clearly demonstrates again that the
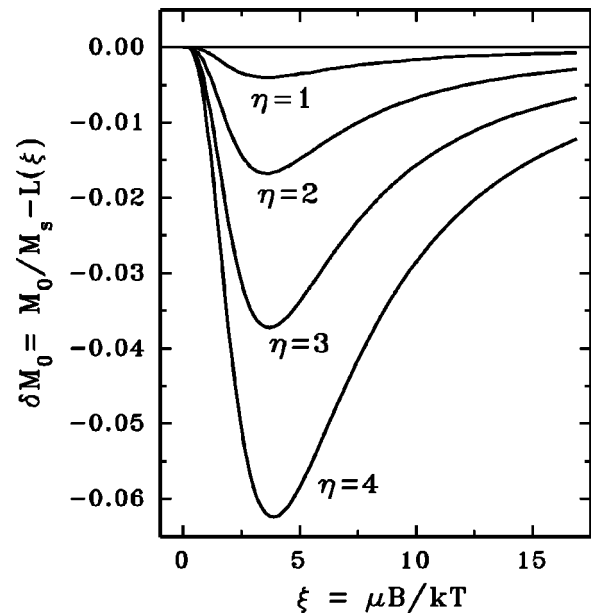

FIG. 1. Departure of the theoretical relative magnetization curve M_0/M_s from Langevin function $L(\xi)$ for different values of the anisotropy parameter η.

initial susceptibility equals that of $L(\xi)$ and, as expected for $\eta = 0$, the magnetization curve is well described by the Langevin function $L(\xi)$, i.e., $\delta M_0 \equiv 0$.

C. Magnetically textured systems

When the particles are frozen in the matrix in the presence of a magnetic field $B_p = b_p B_p$, a nonuniform distribution of the easy magnetization axes is established. Two limiting cases may be considered according to the relative orientations of the field applied in magnetization measurements and during the sample preparation process: (a) *the parallel geometry* ($b \| b_p$), identified by the symbol $\|$ and (b) *the perpendicular geometry* ($b \perp b_p$), identified by the symbol $\perp$. These two configurations have been mentioned in Ref. 7. In the following discussion, and also for the analysis of our experimental results we will concentrate on the *parallel geometry*, which is more interesting from a physical point of view, as explained below.

In the parallel geometry the alignment of magnetic moments for small induction B is favored by the magnetic texture. As a result, the gel sample is magnetized more easily than the corresponding ferrofluid solution and $\delta M_\|$ is positive. When the parameter ξ related to the magnetizing field reaches the value ξ_p proportional to the preparation field, the distribution of anisotropy axes is similar to that of the corresponding ferrofluid solution and $\delta M_\| = 0$ at this point. It should be mentioned that the parameters ξ and ξ_p are also functions of temperature during magnetization and sample preparation experiments, respectively. In our case, both preparation and measurements were performed at room temperature, which means that instead of $\xi = \xi_p$ we could just as well write $B = B_p$. Assuming no ageing process, i.e., no time dependent reorientation of the easy axes in the matrix, we
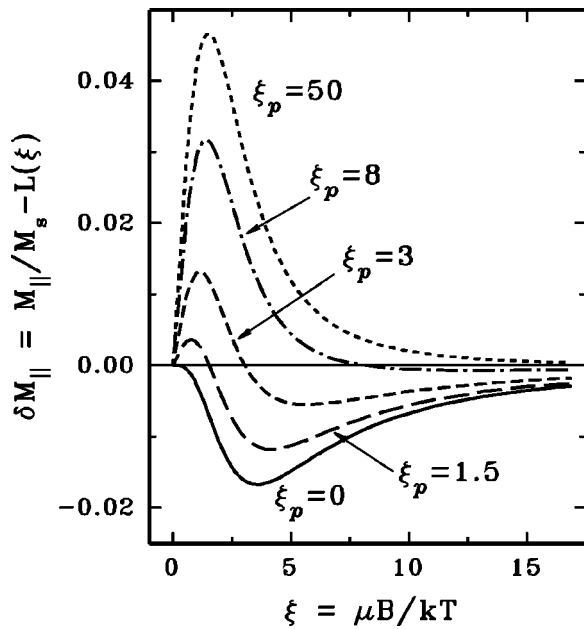
FIG. 2. Difference between the theoretical relative magnetization $M_\parallel/M_s$ and Langevin function $L(\xi)$ for $\eta=2$ for several values of the preparation field parameter $\xi_p=\mu B_p/kT$.

could determine the preparation field value B_p applied during the solidification of the gel.

All these facts are demonstrated in Fig. 2, where the variation of $\delta M_\parallel$ with ξ is plotted for different values of ξ_p at a given η value. The effect of magnetic texturing increases obviously with the preparation field value. The limiting cases are $\xi_p=0$ for which $\delta M_\parallel \leq 0$, as discussed previously, and $\xi_p \gg 0$ where the magnetization becomes easier ($\delta M_\parallel > 0$) in the whole ξ range of interest. For a given ξ_p the absolute value of the difference $\delta M_\parallel$ increases with the parameter η, relating the anisotropy and thermal energies (Fig. 3).
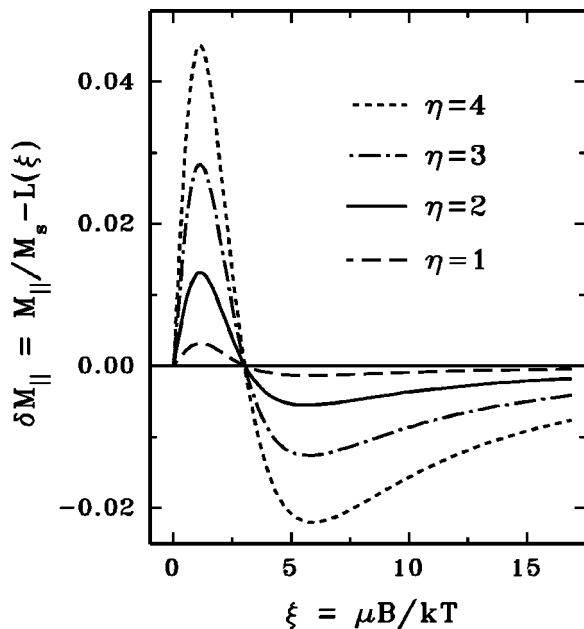

FIG. 3. Variation of $\delta M_\parallel$ with ξ calculated for several values of $\eta = KV/kT$ and for $\xi_p=3$.

D. Polydisperse structures

Real ferrofluid solutions contain magnetic particles with different diameters D and a log-normal distribution $P(D)$ is usually considered in this case[15]

$$P(D)=\frac{1}{\chi D \sqrt{2\pi}}\exp\left(-\frac{(\ln D - \ln D_o)^2}{2\chi^2}\right). \tag{13}$$

A mean diameter D_m and a standard deviation σ can be calculated from D_o and χ using

$$D_m=D_o\exp\left(\frac{\chi^2}{2}\right), \tag{14}$$

$$\sigma=D_m\sqrt{\exp(\chi^2)-1}. \tag{15}$$

As is well known[14,17] the distribution of particle diameters modifies the field induced magnetic response of the system and a weighted sum of contributions from particles with different diameters has to be considered

$$M=\int_0^\infty M(D)P(D)dD. \tag{16}$$

The particle size enters the model employed for explaining the magnetization curves through parameters ξ (or ξ_p) and η. In the case of spherical particles one can write

$$\xi=\xi'D^3B, \quad \text{with} \quad \xi'=\frac{\pi M_{sp}}{6kT}, \tag{17}$$

$$\eta=\eta'D^3, \quad \text{with} \quad \eta'=\frac{\pi K}{6kT}. \tag{18}$$

Here M_{sp} stands for the saturated magnetization of the particle, which is supposed to be identical at all particle diameters. In expressions (17) and (18) we introduced new parameters ξ' and η' independent of the particle diameter and applied field.

III. SAMPLES AND EXPERIMENTAL METHODS

A. Sample preparation

A simple manner to ''freeze'' ferrofluid nanoparticles is to insert them into a solid medium. For this purpose we chose, both for their excellent mechanical and optical properties, to use silica matrices prepared via the sol–gel process. The chemistry involved in this process is based on hydrolysis and condensation reactions of silicon alkoxides, $Si(OR)_4$. Condensation of hydrolyzed species ($\equiv$Si–OH+HO–Si $\equiv$$\rightarrow$$\equiv$Si–O–Si$\equiv$) leads to a silica base gel.[18] After drying at a moderate temperature ($<100\ °C$), the gel is converted into a solid transparent matrix (called ''*xerogel*''). The optical transmission of an undoped silica xerogel in the visible range is similar to that of a glass plate.

If nonreactive species are inserted into the initial solution (called ''sol'') the solid oxide network gradually grows around these species during the sol–gel reaction and finally gives a doped gel with dispersed species encaged in the pores of the gel. In the past 10 years numerous works have been devoted to the properties of doped xerogels, especially to their optical properties.[19] According to the nature of the dop-

ants, gain media for the solid state tunable laser,[20] photochromic materials,[21] photorefractive materials,[22] second harmonic generation materials[23] or media for all-optical memories[24] were prepared. We report here on one of the first attempts to encage the ferrofluid particles into the pores of a silica gel matrix in order to freeze their magnetic moments.

The preparation procedure of the host gel matrices has been described elsewhere.[20] In this study the tetraethoxysilane (TEOS) was used as silicon alkoxide. Hydrolysis and condensation were performed under acid-catalyzed conditions with alcohol as the common solvent. The gel drying was performed in air at room temperature for 2 weeks. A small amount of an ionic aqueous ferrofluid was added after complete hydrolysis. More precisely, the magnetic particles in the ferrofluid are nanocrystals of maghemite, γ-Fe_2O_3, prepared according to the technique developed by Massard.[25] They are ferrimagnetic with a Néel temperature larger than 600 °C. These crystallites present the same inverse spinel structure as magnetite, Fe_3O_4. Each particle bears a negative electric charge. The addition of a commercial surfactant (EMCOL CC59) containing cationic counter ions allows one to stabilize the colloidal suspension of nearly spherical maghemite particles in a mixture of water and isopropanol.

Starting from samples containing the same volume fraction of γ-Fe_2O_3 particles as in the gel matrix, three types of magnetic textures were realized. For the first type ''N'' (for ''no field'') the solution was solidified in the absence of any applied magnetic field to generate an isotropic distribution of the easy anisotropy axes of the particles. For the second type ''I'' (for ''in-plane field'') or third type ''O'' (for ''out-of-plane field'') the solution was solidified between the pole pieces of a permanent magnet. The preparation magnetic field with induction $\boldsymbol{B}_p$ ($B_p = 0.124$ T) was applied in the plane (''I'') or perpendicular to the plane (''O'') of the gel platelet. Typical thicknesses of these platelets are in the range 0.3–0.5 mm.

B. Structural and chemical characterization by electron microscopy

Transmission electron microscopy (TEM) carried out in different imaging modes allows one to check the sample morphology, i.e., the size and shape distributions of the magnetic nanoparticles, and to evaluate their separation. Additional investigations by energy dispersive x-rays spectroscopy (EDXS) and electron energy loss spectroscopy (EELS) give information on the elemental composition and the volume fraction of the particles. EDXS and EELS are based, respectively, on radiative deexcitation effects and on transitions to unoccupied states, leading to an energy loss for the transmitted electrons. Chemical bonding, electronic structure and local order could be checked by EELS as in x-ray absorption spectroscopy.[26]

Two microscopes were mainly used in our studies. The first one was a 200 keV ''classical'' TEM TOPCON 002B equipped with EDXS and parallel EELS detectors. The second one was a 100 keV ''dedicated'' scanning TEM VG HB 501 (STEM), equipped with a specific EELS spectrometer[27] and with image detectors for collecting transmitted electrons at different scattering angles, in particular in bright field (BF)
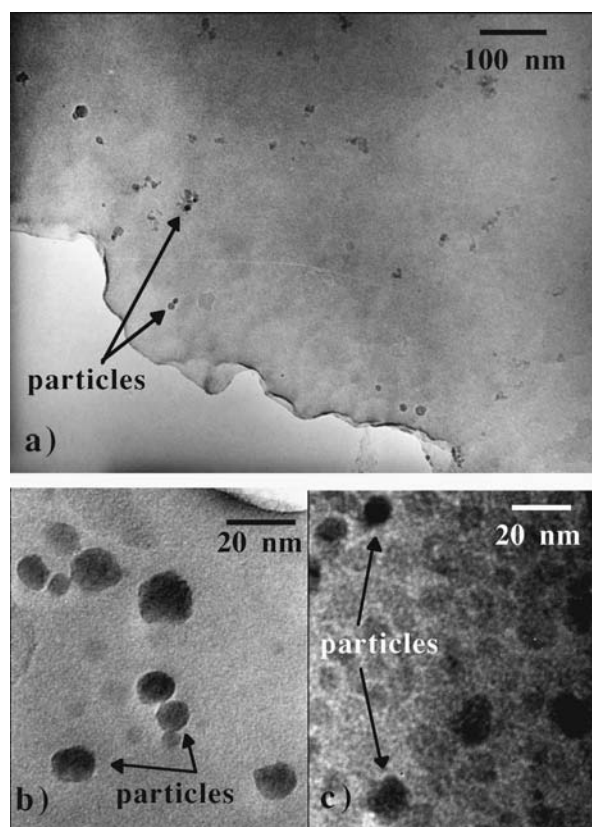

FIG. 4. TEM-BF images of gel specimens: (a) type ''N'' (''no field'') sample, general view and (b) local view, (c) type ''I'' (''in-plane field'') sample, local view. Images (b) and (c) were acquired by a charge-coupled device (CCD) camera on the TEM TOPCON 200 keV.

and high angle annular dark field (HAADF) modes. Owing to the fact that usual ion milling was unsuitable to thin down such a type of xerogel matrix, the experiments were carried out on very small wedge pieces of matter cut along an appropriate direction in the case of textured samples.

In the morphological study of the gel specimens, it was important to check first that the observed objects were really γ-Fe_2O_3 particles and also to locate precisely the boundary of each particle to determine accurately the particle size and shape distributions. In order to distinguish the maghemite particles in the matrix from other sources of contrast on TEM-BF images (Fig. 4), a local chemical analysis has been performed simultaneously by EDXS and EELS, using an electron beam diameter as small as 10 nm. Especially on the ''I'' gel specimen, the local TEM-BF contrast in several areas of the SiO_2 matrix could be mistaken for that due to the particles [Fig. 4(c)]. In fact, the BF contrast depends strongly on structural effects, specimen mass thickness, wave interferences, etc. In other respects, STEM-HAADF performed at high angles (>30 mrad) allows one to locate precisely the γ-Fe_2O_3 particles over large specimen areas (typically between 20×20 and 1000×1000 nm^2) and with thickness up to several hundreds nanometers. It stands as a powerful method since the contrast is highly dependent on the local atomic number Z. In this mode, the particles in the thickest areas appear in dark (Fig. 5) while the contrast is inverted in the thinnest parts.
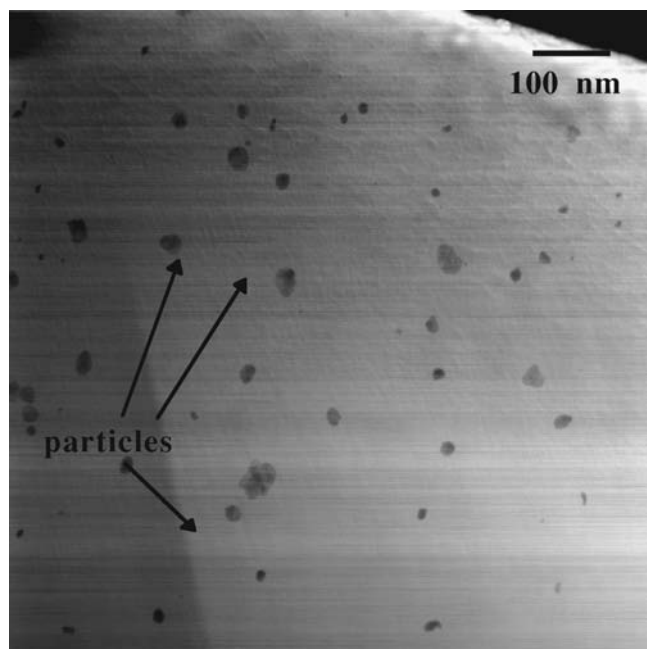
FIG. 5. HAADF image of the gel specimen ''I'' (''in-plane field'') acquired on the STEM VG 100 keV.
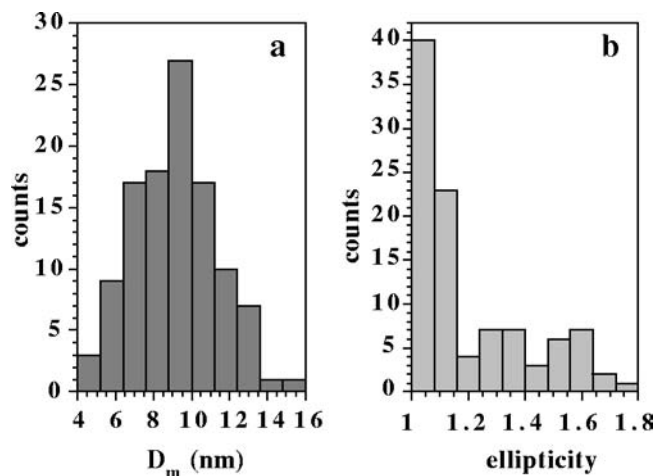

FIG. 6. Examples of (a) particle size and (b) particle ellipticity distributions in the dried ferrofluid. Morphology analysis was realized on STEM-BF images.

The determination of the particle size distribution was critical. Thus, two significantly different threshold methods were used and compared. In the first method [''auto'' (A)], the threshold value was chosen to optimize the binary operation, whereas in the second one [''manual'' (M)] each individual particle image was fitted by appropriate circular or ellipsoidal shapes. In both cases, one tried to eliminate, as systematically as possible, the areas where the particles are superposed in depth. The magnification given by the two microscopes was accurately calibrated from a standard catalase crystal.

The particle size distribution characteristics, determined in different imaging modes, are presented in Table I for the

TABLE I. Mean diameter D_m and the standard deviation σ for assemblies of n γ-Fe_2O_3 particles in the dry ferrofluid or embedded in the type ''N'' or ''I'' samples, compared with values determined from magnetic measurements. The results, obtained at different TEM or STEM modes and with (A) or (M) threshold methods are compared. For the gels, the low σ value in the TEM-BF mode comes probably from the examination of a too limited number of particles.

Imaging mode (threshold method)	D_m (nm)	σ (nm)	n
Dried ferrofluid solution			
TEM-BF (A)			
STEM-BF (A)	9.1±0.9	3.8	289
STEM-BF (M)	9.8±0.9	1.9	100
STEM-HAADF	10.7±1.3	5.5	447
(A and M)			
Ferrofluid-fit of the magnetization curve			
—	10.5±1.1	4.6±0.6	
Type ''N'' and ''I'' gels			
TEM-BF (A)	15.0±1.5	4.9	46
STEM-HAADF (A)	17.3±1.7	7.0	358

initial ferrofluid after evaporating the solution, as well as for the ''N'' and ''I'' types of specimens. The mean diameter values D_m for different assemblies of n particles and their standard deviations σ are reported there. D_m values are determined from the particle areas, assuming their spherical shape. The error bars on D_m (Table I) are estimated from the dispersion of ten measurements on the same particle using the manual threshold method (M).

For the ferrofluid, all D_m values determined by STEM-BF and STEM-HAADF are close together (Table I). As mentioned above, the HAADF image contrast, checking directly the atomic number of the elements, appears more relevant for a precise determination of the D_m absolute value. This is also supported by the fact that the A and M threshold methods give exactly the same results in HAADF. We are also confident with the measured particle size distribution since it does not depend much on the imaging mode for large assemblies of n particles. The D_m distribution, measured in the STEM-BF mode, is depicted in Fig. 6(a). The agreement between the D_m and σ values, deduced either from further magnetic measurements or from the STEM-HAADF experiments is remarkable (Table I). The typical particle ellipticity distribution deduced from the STEM-BF image of an assembly of dried ferrofluid particles is presented in Fig. 6(b). Then, with the ellipticity being rather small, it is *reasonable to assume* in the following magnetic study (Sec. IV C) that one deals with *spherical particles*.

In counterpart, for the frozen particles in the gel, the D_m values deduced for the ''N'' and ''I'' specimens from the two TEM-BF and STEM-HAADF image modes (D_m =15 nm and 17.3 nm, respectively) are unexpectedly overestimated since there is no fundamental reason to determine values which differ from those corresponding to the dried ferrofluid (9.1–10.7 nm). This disagreement has certainly several origins: the multiple electron scattering, the ''top-bottom'' effect due to the spatial location of the particles inside the thin platelet relative to the objective lens position[28] and the fact that some particles tend to group together (Fig. 4). The closeness between particles, associated with a beam

TABLE II. Local and global chemical electron microscopy analysis. In the local analysis, the EDXS and EELS are measured simultaneously on the same individual particle area. The global analysis corresponds to an average of ten (for TEM) or 20 (for SEM) measurements on nonoverlapping sample volumes and at different scales.

Analytical method	Edges	Gel: type ''N'' (no preparation field)	Gel: type ''I'' (in-plane field)
		Local analysis–beam size 10 nm (in at. %)	
TEM-EDXS	Si_K	21.9 ± 0.6	25.2 ± 0.6
(on a particle)	O_K	62.3 ± 5.0	63.9 ± 5.0
	Fe_K	15.8 ± 0.5	10.8 ± 0.5
TEM-EELS[a]	$Si\ L$	21.5 ± 1.0	—
(on a particle)	$O\ K$	62.0 ± 3.0	—
	$Fe\ L$	16.5 ± 1.2	—
TEM-EDXS	Si_K	32.0 ± 1.0	34.8 ± 1.0
(out of	O_K	68.0 ± 3.0	65.2 ± 3.0
particles)	Fe_K	<0.1	<0.1
		Global analysis (in at. %)	
TEM-EDXS	Si_K	34.6 ± 1.0	31.1 ± 1.0
(total analyzed	O_K	65.1 ± 3.0	68.2 ± 3.0
volume: 20 μm^3)	Fe_K	0.30 ± 0.04	0.61 ± 0.07
SEM-EDXS	Si_K	35.6 ± 1.7	35.4 ± 1.6
(total analyzed	O_K	64.1 ± 5.0	64.2 ± 5.0
volume: $2 \times 10^3\ \mu m^3$)	Fe_K	0.30 ± 0.09	0.38 ± 0.11

[a]Acquired simultaneously with TEM-EDXS.

broadening effect, leads to an overestimation of their mean diameter. This explanation is also supported by the fact that the experimental distributions of particle diameters and ellipticities spread more for the gel samples than in the dried ferrofluid. In the present experimental conditions, we are more confident with the D_m and σ values obtained for the evaporated ferrofluid. This study demonstrates that a more precise determination of the size of particles embedded in gels needs an originally prepared thin film specimen.

As mentioned above, the local chemical composition of the samples has been checked by EDXS and EELS in the ''N'' and ''I'' specimens. These two high resolution methods were often used simultaneously and typical results are reported in the ''local analysis'' part of Table II. The calibration for each type of spectroscopy was performed using standard samples (SiO_2 and Fe_2O_3, Fe_2SiO_4) and different characteristic signals (O_K, Si_K, Fe_K in EDXS and Si-L, O-K and Fe-L in EELS).[29,30] The photon absorption correction was done in EDXS[31] considering the thickness estimated by EELS[32] and the experimental value of the electron mean free path.[33] The local atomic composition in particle regions provided by EELS and EDXS are close together and confirm the consistence between the two TEM analysis modes (Table II). The atomic composition of the matrix determined out of the particle regions is obviously that of SiO_2. The EELS fine structures, acquired for the gel matrix and for the ferrofluid particles on Si-L, Fe-L inner shells, are unambiguously assigned to SiO_2 and γ-Fe_2O_3, respectively.[34]

After looking at individual particles, the global mean composition TEM-EDXS and EELS analysis over a large specimen volume was performed in order to deduce the volume fraction Φ of γ-Fe_2O_3 particles and for checking the homogeneity of their spatial distribution (Table II). The TEM-EDXS reported values are an average over ten inde-

pendent measurements on nonoverlapping small regions of the specimen; the total volume investigated is therefore estimated to about 20 μm^3. For the investigation of larger volumes, bulk specimens were studied directly using a scanning electron microscope (SEM) working at 15 kV. In that case, the results reported in Table II represent the average of 20 measurements which cover about $2 \times 10^3\ \mu m^3$ of matter. Even at this scale, the dispersion of Fe composition is quite large. In spite of such a dispersion, a good agreement between the global TEM and SEM sample analyses was obtained for the type ''N'' sample (Table II). The heterogeneity of the γ-Fe_2O_3 particle distribution is higher in the analyzed ''I'' specimen, as revealed by the far larger difference between Fe composition values when increasing the probed volumes. With the global chemical analysis giving the relative mass concentration, one can deduce the volume fraction Φ using the matrix density $\varrho = 2 \times 10^3$ kg m^{-3}, which assumes a very low porosity of the matrix. From the analysis of a quite large specimen volume of about 10^{-4} mm^3 by SEM-EDXS one gets $\Phi = (0.43 \pm 0.13)\%$ and $\Phi = (0.60 \pm 0.16)\%$, respectively, for the ''N'' and ''I'' samples. The above values of Φ, deduced from electron microscopy, are slightly larger than those extracted from the following magnetic measurements (Sec. IV B). Note that the reported errors on Φ (Table II) do not take into account the large inhomogeneity of the particle distribution in the specimen, especially revealed for the type ''I'' sample. In magnetic measurements we are probing much bigger volumes (typically some mm^3) so that the observed differences between the Φ values may be related to the sample heterogeneity at relatively large scales.

Let us finally note that no preferred alignment of the particles along the preparation field direction has been evidenced for the ''I'' type of sample (Fig. 5). The surfactant plays certainly an important role for avoiding the coalescence and ordering between magnetic particles under a static magnetic field during the sol–gel reaction. The particles were uniformly distributed in both ''N'' and ''I'' specimens (Figs. 4 and 5). The mean distance between the neighboring groups of particles (or between isolated particles) was about (150 ± 40) nm. The mean distance between the particle centers inside groups was (50 ± 15) nm (Fig. 4), i.e., a typical length which avoids strong magnetic coupling by dipolar forces.[35] Thus, in the following magnetic treatment, the *particles* will be considered as *magnetically isolated*.

C. Magnetic measurements

Room temperature magnetization measurements were performed with an alternating gradient force magnetometer[36] (Micro Mag 2900, Princeton Measurements Corporation). Two different probes were used for measurements in a field **B** applied in the plane or perpendicular to the plane of the sample platelet. The diamagnetic contribution of the probes and of the gel matrix were substracted from the full magnetization signal. The diamagnetic susceptibility of the matrix was equal to -5.4×10^{-3} A m^2 kg^{-1} T^{-1}, i.e., an usual value for glass. In our samples the diamagnetic contribution of the matrix at the maximum applied field ($B = 1.9$ T) rep-

resents about 2.6% of the total magnetization of the sample. With our experimental setup we were able to measure the magnetization of the gel samples but not that of the ferrofluid because of the too large contribution of the container. For $B = 1.9$ T the measured specific magnetization M_s' of the studied gel samples was

$$M_s' = (0.38 \pm 0.01) \text{A} \ \text{m}^2 \text{kg}^{-1} \tag{19}$$

(or 0.38 emu/g). This value will be considered as their magnetization at saturation.

Since the samples were small enough ($\sim 1 \times 1 \text{ mm}^2$), with a mass of about 3 mg, the inhomogeneity of the field gradient applied on the sample can be neglected. We consider that all spurious effects were well eliminated since the resulting saturated magnetizations differ only within 2.6% in spite of a large variation (100%) of the mass of the sample pieces. This remark is very important when looking at small differences on magnetization curves, as in our case. We verified that the in-field magnetization curves can be well rescaled with the concentration of particles frozen in the matrix around the studied composition. This confirms that our samples contain only a negligible amount of aggregates with strongly interacting magnetic particles.

D. Magneto-optical measurements

Magneto-optical effects were widely used to measure the magnetization and the magnetic anisotropy in ferrofluids.[15,37] We report here on room temperature magnetic circular dichroism measurements of the magnetization in light transmission which give the Faraday ellipticity ϵ_F. The measurement of ϵ_F was preferred to that of the Faraday rotation to avoid the background due to the magneto-optical rotation by the container or the transparent matrix. Magnetic linear birefringence and dichroism, proportional to the square of magnetization, are also reported in this study.

Details on the used magneto-optical arrangement at fixed photon energies have been described elsewhere.[38] Sensitive measurements based on the modulation of the ellipticity of light at high frequency $f_m \approx 50$ kHz are performed through a lock-in detection technique. In polar configuration $\boldsymbol{B} \| \boldsymbol{\gamma}$ ($\boldsymbol{\gamma}$ being the light wave vector), the magnetic circular dichroism is detected at the f_m frequency. Magnetic linear dichroism (MLD) is measured at the $2f_m$ frequency in the transverse or Voigt–Cotton–Mouton configuration ($\boldsymbol{B} \perp \boldsymbol{\gamma}$). A liquid nitrogen cooled coil was used to generate a field ($B \leqslant 0.3$ T) with a very good homogeneity. The magneto-optical experiments were performed at the green He–Ne laser line ($\lambda = 543.5$ nm).

Let us discuss briefly the proportionality between the Faraday ellipticity, proportional to the imaginary part of the complex circular birefringence ΔN_c, and the M_γ component of the magnetization. For a polydisperse assembly of particles, ΔN_c can be expressed by $\Delta N_c = \int_0^\infty \Delta N_c(D) P(D) dD$. Considering that the optical properties of the matrix with embedded particles, which are not strictly spherical, depend on the orientation of the particles
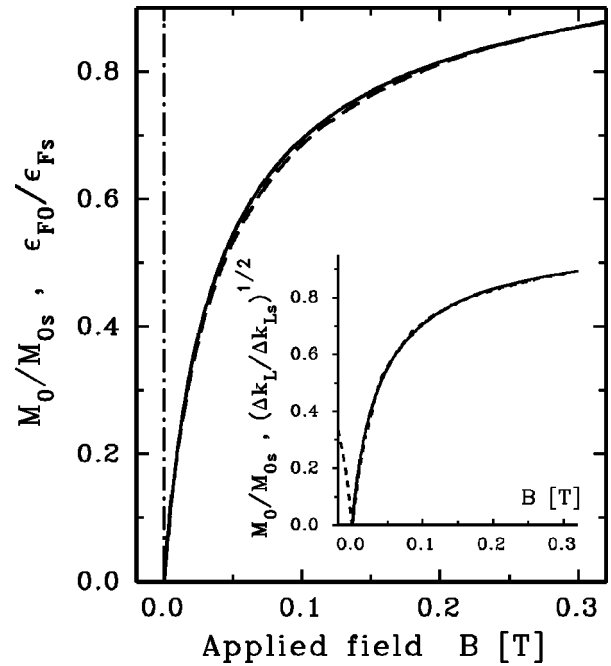

FIG. 7. Magnetization curve of a gel sample with a uniform distribution of anisotropy axes (type ''N'' sample) measured using AGFM (solid line) compared with the magnetic field dependence of magneto-optical quantities (dashed lines) measured at $\lambda = 543.5$ nm: Faraday ellipticity (main graph) and the square root of magnetic linear dichroism Δk_L (inset).

and that ΔN_c may depend on D, the proportionality of ϵ_F to the polar magnetization component of the particles can be affected.

Thus, we compared the field dependence of the normalized magnetization M/M_s with the normalized Faraday ellipticity ϵ_F/ϵ_{Fs} (ϵ_{Fs} is the saturation value) for all samples N, I and O. As an example, Fig. 7 shows this comparison for the type ''N'' sample. Because the Faraday ellipticity measurements were restricted to fields up to $B = 0.3$ T, the Faraday ellipticity curve is normalized such as $M_0(0.3 \text{ T})/M_{0s} = \epsilon_{F0}(0.3 \text{ T})/\epsilon_{F0s}$. Reasonably weak differences, smaller than 1.5% of the saturation value, are noticed between the two curves. Such differences were, within our experimental error, practically identical for all samples (N, I and O). The expected magnetization curve of the ferrofluid solution was consequently deduced from the Faraday ellipticity measurement. A similar agreement was found between the in-field magnetization curve and the square root of the magnetic linear dichroism $\Delta k_L/\Delta k_{Ls}$ (which is expected to vary as the square of the in-plane magnetization component) for the type ''N'' sample (inset of Fig. 7).

In the following we will restrict ourselves to the analysis of the magnetization and Faraday ellipticity curves up to $B = 0.3$ T. This 0–0.3 T range is well adapted to demonstrate significant magnetic properties of our textured superparamagnets.

IV. MAGNETIZATION: EXPERIMENTAL RESULTS AND DISCUSSION

A. Generalities

The aim of this section is to compare the experimental data of in-field magnetization for γ-Fe$_2$O$_3$ particles frozen in

the gel matrix to that obtained for the reference ferrofluid solution and to discuss the results in the framework of the previous theoretical considerations (Sec. II).

Thus, we will first determine the pertinent parameters of our assembly of polydisperse particles which will be subsequently frozen in the matrix. Then we will analyze the differences between relative magnetizations

$$\Delta M_i = \frac{M_i}{M_{is}} - \frac{M_f}{M_{fs}} \qquad (20)$$

and Faraday ellipticities

$$\Delta \epsilon_{Fi} = \frac{\epsilon_{Fi}}{\epsilon_{Fis}} - \frac{\epsilon_{Ff}}{\epsilon_{Ffs}} \qquad (21)$$

for gel samples prepared in the absence or presence of a magnetic field B_p and for the ferrofluid. Here the subscripts i will be 0 for type ''N'' sample ($B_p=0$), $\parallel$ ($\perp$) when the applied field is parallel (perpendicular) to the preparation field, while f refers to the ferrofluid.

Because of lack of Faraday ellipticity data at fields larger than $B=0.3$ T, the exact saturation values ϵ_{Fis} as well as ϵ_{Ffs} and also M_{fs} were not available. We have found that the analysis of the experimental data for magnetic fields $B \leq 0.2$ T is still valid if the magnetization curves are rescaled at $B=0.3$ T with a relative magnetization (or Faraday ellipticity) value of 0.87, which was measured by magnetometry for the type ''N'' sample. The magnetization curves rescaled to this value provide quantities ΔM_i and $\Delta \epsilon_{Fi}$ which tend to zero at $B=0.3$ T. Thus, we gave up the part of ΔM_i and $\Delta \epsilon_{Fi}$ describing the behavior of our samples at higher fields. Furthermore, the most useful part of the magnetization curves is restricted to fields $B<0.15$ T, where the experimental differences ΔM_i and $\Delta \epsilon_{Fi}$ are only negligibly modified by the scaling.

Now, we will determine first the pertinent parameters necessary to fit the ferrofluid magnetization curve, i.e., for an assembly of polydisperse γ-Fe$_2$O$_3$ particles which will be subsequently frozen in the matrix. We will find the parameters of the size distribution (D_m and σ) as well as the particle saturated magnetization (M_{sp}). Then, from ΔM_0 and $\Delta \epsilon_0$ [expressions (20) and (21)], measured for frozen particles with randomly distributed anisotropy axes (type ''N'' sample), the anisotropy constant K will be determined. Third, we will report on the precise $\Delta M_{\parallel}$ ($\Delta \epsilon_{F\parallel}$) and $\Delta M_{\perp}$ ($\Delta \epsilon_{F\perp}$) variations for magnetically textured gel samples. These results will be discussed from calculations.

B. The ferrofluid solution

The normalized magnetization curve (Fig. 8) of the ferrofluid can be well fitted by expression (16), where $M(D)$ is proportional to the Langevin function (7) and $P(D)$ is taken as a log-normal distribution (13). From the fit we got $D_0=(9.6\pm1)$ nm, $\chi=(0.42\pm0.02)$ and $\xi'=(3.5\pm0.4)\times10^{25}$ T^{-1} m^{-3} [ξ' is defined by expression (17)]. From D_0 and χ one deduces the mean particle diameter $D_m=(10.5\pm1.1)$ nm and the standard deviation $\sigma=(4.6\pm0.6)$ nm of the expected distribution of particle diameters. These values, deduced from our magnetic data, are in a perfect agreement
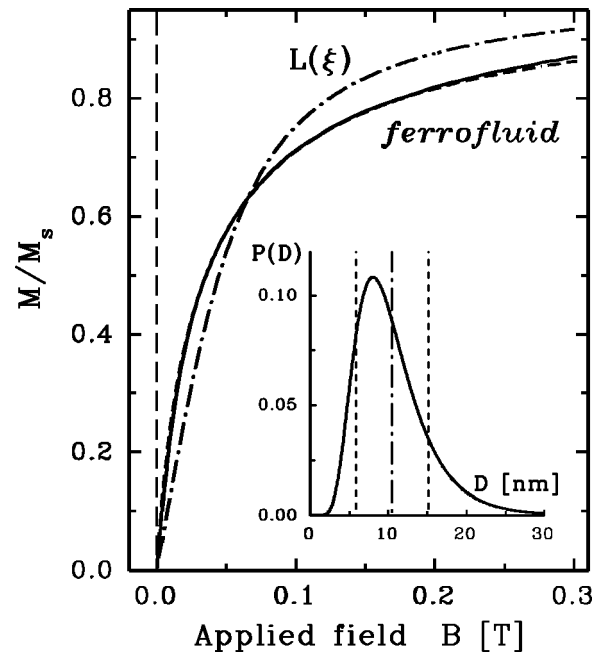

FIG. 8. Magnetization curve of the ferrofluid: experiment (full line), fit (dashed line) and Langevin curve calculated for a monodispersed solution with $D=D_m=10.5$ nm (dash-dot line). The inset plots the $P(D)$ density for a log-normal distribution [expression (13)] deduced from a fit of the magnetization curve. The vertical dash-dot line marks the mean diameter $D=D_m$ of particles, whereas the vertical dashed lines are located at $D=D_m-\sigma$ and $D=D_m+\sigma$.

with those obtained from TEM and STEM structural studies (Table I), in particular, if one assumes that the STEM-HAADF results are more relevant. In Fig. 8 we also plotted the Langevin curve computed for a monodispersed solution with the above D_m and ξ' values, which departs significantly from the data. This proves that without considering the distribution of particle diameters it is not possible to fit reasonably our experimental data. As theoretically predicted[8] for polydisperse magnetic particles, the low field susceptibility is higher than that given by the Langevin function (Fig. 8).

From parameter ξ' [expression (17)] one can deduce the saturated magnetization value of particles: $M_{sp}=(2.8\pm0.3)\times10^5$ A m^{-1} [or in centimeter-gram-second (cgs) system $4\pi M_{sp}=3500$ G]. This result corresponds within the experimental accuracy to the value $4\pi M_{sp}=(3400\pm500)$ G reported by Bacri *et al.*,[15] who also observed that M_{sp} was independent of the particle diameter. Such a value is 24% lower than the magnetization of bulk γ-Fe$_2$O$_3$. As discussed in Ref. 15, this decrease of magnetization can be explained by a lack of magnetic ordering in a thin layer on the particle surface. In our opinion it can be also partly due to the fact that the real distribution of particle diameters [Fig. 6(a)] differs somewhat from the considered log-normal distribution (inset of Fig. 8).

Knowing the specific sample magnetization value M'_s [Eq. (19)], the density ϱ of the matrix ($\varrho=2\times10^3$ kg m^{-3}), and the particle magnetization M_{sp}, it is straightforward to deduce the volume fraction Φ of the particles in the matrix, $\Phi=0.28\%$, for both types of samples.
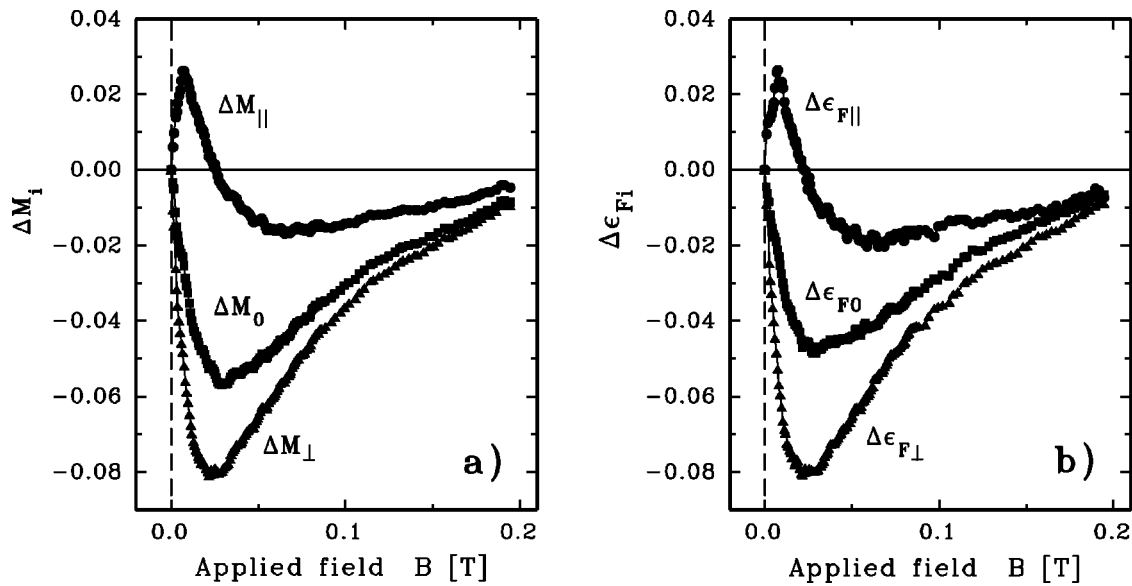
FIG. 9. Excess of the relative magnetization (a) and Faraday ellipticity (b) as a function of the applied field B with respect to the ferrofluid solution for the gel samples prepared in the absence of external magnetic field (ΔM_0, $\Delta \epsilon_{F0}$-squares) and synthesized in magnetic field with induction $B_p = 0.124$ T and measured in parallel $\boldsymbol{B} \| \boldsymbol{b}_p$ ($\Delta M_\|$, $\Delta \epsilon_{F\|}$-circles) and perpendicular $\boldsymbol{b} \perp \boldsymbol{b}_p$ ($\Delta M_\perp$, $\Delta \epsilon_{F\perp}$-triangles) configurations.

C. The type ''N'' sample

In this case the anisotropy axes are randomly oriented in all directions, since the spin structure was frozen in the absence of a magnetic field.

The field dependence of the ΔM_i and $\Delta \epsilon_{Fi}$ differences [expressions (20) and (21)] with the applied field are depicted in Figs. 9(a), and 9(b). Both magnetization and Faraday ellipticity measurements provide similar results, which look similar to theoretical ones,[7] obtained for the monodispersed case (Figs. 1–3). In particular, ΔM_0 and $\Delta \epsilon_{F0}$ are always negative, i.e., the sample ''N'' is more difficult to magnetize than the ferrofluid under field, as demonstrated by Raikher.[7] At low field, the experimental differences ΔM_0 and $\Delta \epsilon_{F0}$ depart from zero more rapidly than expected theoretically [$\delta M_0(\xi)$ curves] for a gel with monodispersed particles (Fig. 1). This again shows that the distribution of particle sizes has to be taken into account for fitting the data reasonably. The difference $\delta M_0(B)$ rapidly rises with the particle diameter (Fig. 10). Similarly to the magnetization of polydisperse ferrofluid solutions, one observes here that bigger particles display a stronger δM_0 variation at low field B. The average calculated variation $\delta' M_0(B)$ for our particle distribution is plotted in Fig. 11 for a log-normal distribution with $D_m = 10.5$ nm and using two different values of the standard deviation $\sigma = 3.2$ and 4.6 nm and two values of the anisotropy constant K. A reasonably good agreement with the experimental field variation of ΔM_0 and $\Delta \epsilon_{F0}$ (Fig. 11) is achieved for $K = K_0 = 1.8 \times 10^4$ J m^{-3}, a value close to that found in Ref. 39. It is about four times larger than that reported for bulk material,[15] but consistent with the value $K = 6.4 \times 10^4$ J m^{-3}, recently obtained on the same type of sample with $D_m = 7$ nm at low temperature.[40]

D. Magnetically textured samples

During solidification of the matrix under magnetic field B_p a certain degree of orientational spin texture is frozen-in.

Since in our case the spin reversal is very fast because of the small value of $\eta = kV/kT \ll 25$,[14] the application of the field first selects preferentially a ''speromagnetic'' spin configuration of the particles in one hemispheric space region. The equilibrium distribution $f(\boldsymbol{n})$ of the particle easy axes $\boldsymbol{n}$ results from the balance between the Zeeman (μB_p), anisotropy (KV) and thermal (kT) energies which takes into account the effects of spatial and thermal disorders. The degree of orientational texture is obviously an increasing function of
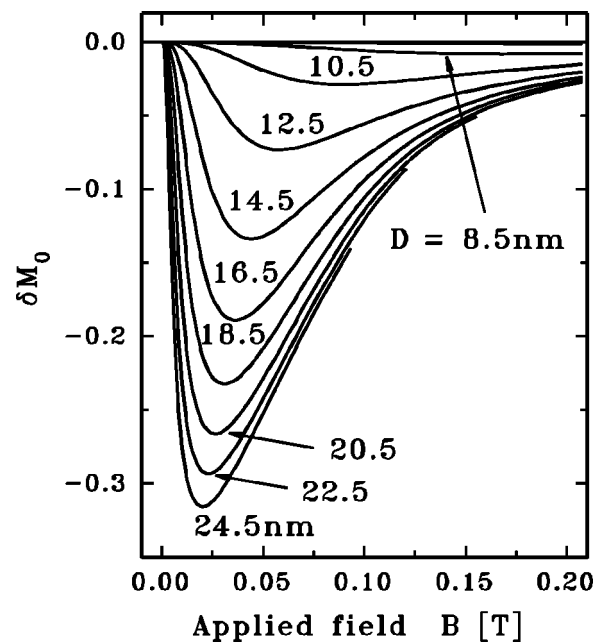

FIG. 10. Difference δM_0 between the relative magnetization curve of monodispersed superparamagnetic particles fixed with uniformly distributed anisotropy axes and the corresponding Langevin function. The calculation has been performed for different particle diameters D, considering a magnetization factor $\xi' = 3.5 \times 10^{25}$ T^{-1} m^{-3} and an anisotropy constant $K = 1.8 \times 10^4$ J m^{-3}.
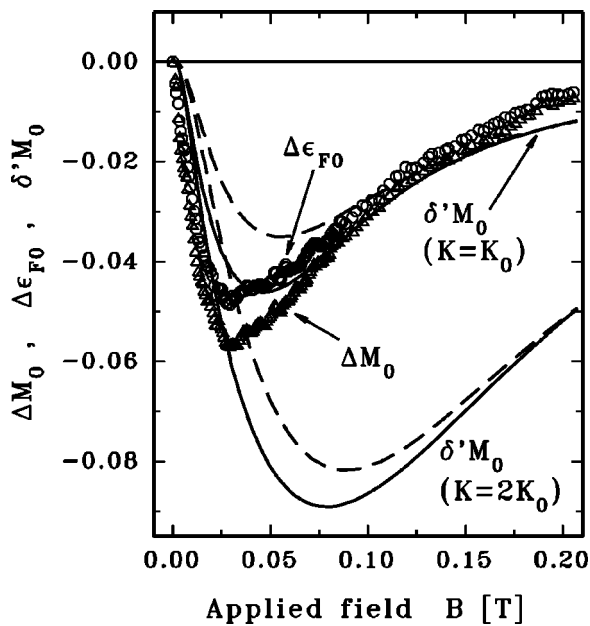
FIG. 11. Experimental differences ΔM_0 (triangles) and $\Delta \epsilon_{F0}$ (circles) compared with the model $\delta' M_0$ (lines) calculated for two values of the anisotropy constant K (with $K_0 = 1.8 \times 10^4$ J m^{-3}) considering a log-normal distribution of particle diameters with the mean diameter $D_m = 10.5$ nm. Solid lines were calculated for a standard deviation $\sigma = 4.6$ nm while dashed lines for $\sigma = 3.2$ nm to demonstrate the effect of σ.

B_p. Because the texture increases with η, the contribution of particles with larger diameters is more efficient than in the previous case of randomly distributed anisotropy axes.

By magnetometry we measured the $M_\parallel$ ($\mathbf{b} \| \mathbf{b}_p$) and $M_\perp$ ($\mathbf{b} \perp \mathbf{b}_p$) magnetization curves for the I-type sample for two orientations of the specimen with respect to the field applied in the plane of the sample. On the other hand, Faraday ellipticities $\epsilon_\parallel$ and $\epsilon_\perp$ were measured on the O-type and I-type samples, respectively. The $\Delta M_\parallel(B)$, $\Delta \epsilon_{F\parallel}(B)$ and $\Delta M_\perp(B)$,

$\Delta \epsilon_{F\perp}(B)$ variations are plotted in Figs. 9(a), and 9(b). For a monodispersed sample it has been already demonstrated in Sec. II, that $\delta M_\parallel$ is positive at low fields and changes sign for $\xi \sim \xi_p$ (Fig. 3). This behavior is still valid for a polydisperse sample (Fig. 9).

Our experimental data $\Delta M_\parallel$ and $\epsilon_{F\parallel}$ are compared in Fig. 12(a) with theoretical curves of $\delta M_\parallel$ for particles having a fixed diameter $D = D_m$ and for three preparation field values B_p. Similar to the case of an isotropic distribution of anisotropy axes we observe that the theoretical model with monodispersed particles cannot explain the observed experimental dependence of $\Delta M_\parallel$ and $\Delta \epsilon_{F\parallel}$ with the applied magnetic field.

The theoretical fit of the data becomes again possible when the model takes into account the particle diameter dispersion, as shown in Fig. 12(b). A reasonable agreement between the theoretical and experimental curves can be obtained for $B_p = 0.025$ T, which is only about 20% of the preparation field induction. This reduction probably comes from ageing effects due to slow time dependent reorientation of the particles in the matrix after the gel solidification. Such relaxation has been clearly evidenced in similar samples by measuring the linear birefringence as a test of the degree of magnetic texture in the sample.[3]

Finally, in Fig. 13 we plotted the difference $M_\parallel / M_{\parallel s} - M_0 / M_{0s}$ between two magnetization curves measured on the magnetometer. These data are both recalibrated to the saturated magnetization (i.e., with no restrictions at $B = 0.3$ T). The shape of the experimental curve is in a very good agreement with the prediction of the theoretical model, even at large fields. The amplitude of this difference corresponds to $B_p \approx 0.04$ T, which is somewhat larger than the value estimated from Fig. 12(b). This difference is reasonable and its source is the same as that already observed between the theoretical and experimental curves in Fig. 11.
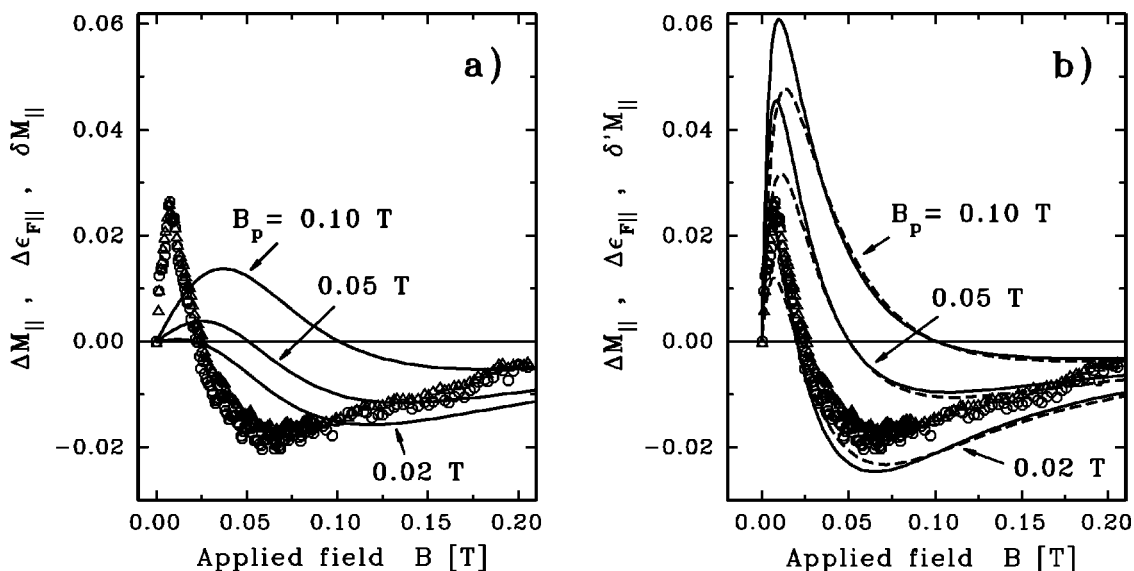

FIG. 12. Experimental variation of $\Delta M_\parallel$ (triangles) and $\Delta \epsilon_{F\parallel}$ (circles) with the applied field B compared with theoretical curves $\delta M_\parallel$ ($\delta' M_\parallel$) for a preparation field B_p calculated (a) for an assembly of identical particles having the diameter $D = 10.5$ nm (full lines) and (b) for particles with diameters distributed according to log-normal law with $D_m = 10.5$ nm and $\sigma = 4.6$ nm (full lines). In order to show the effect of σ on the expected variation of $\delta' M_\parallel$ in the graph (b) we also included curves for $\sigma = 3.2$ nm (dashed lines). The calculations have been made for the anisotropy constant $K = 1.8 \times 10^4$ J m^{-3}.

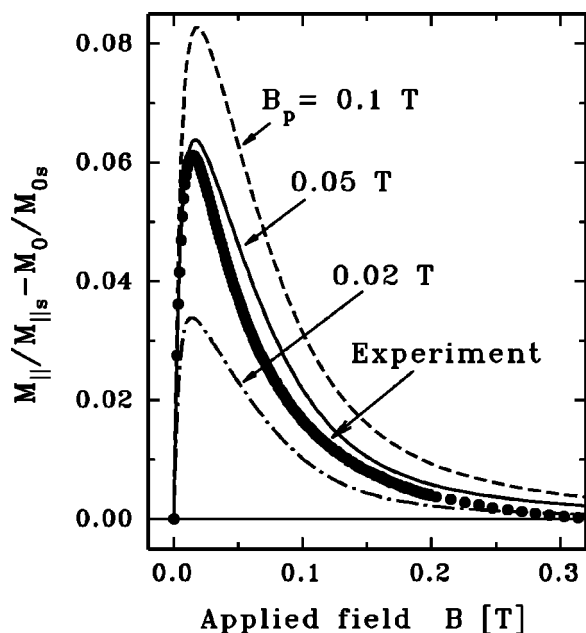J. Appl. Phys., Vol. 83, No. 12, 15 June 1998

Bentivegna *et al.* 7787

FIG. 13. Difference $M_\parallel/M_{\parallel s} - M_0/M_{0s}$ as a function of the applied magnetic field: experimental AGFM data (circles) and theoretical curves for three values of the preparation field B_p (lines).

This is probably a consequence of the fact that the distribution of particle diameters in our samples [Fig. 6(a)] departs from the usually considered log-normal distribution. Another reason is a possible contribution of the shape anisotropy of the particles, which was neglected in this model.

V. CONCLUSIONS

Magnetically textured systems, such as oriented ferrofluid particles embedded in polymers or glasses, are very promising materials for future original applications. In this paper we have reported a refined analysis of the anisotropic magnetic properties of maghemite particles frozen in a gel matrix at orientations adjusted in a magnetic field applied during the solidification process. The morphological and structural information extracted from our electron microscopy measurements allowed us to determine all pertinent parameters, such as the dispersion of particle diameters, their volume concentration, typical shape and their separation, which are relevant in the description of our magnetic results. Starting from the magnetometry data, we proved that magneto-optical ellipticity measurements allow one to determine perfectly the variation of the magnetization in this material when prepared in the absence of a magnetic field. This made possible an accurate comparison of the in-field magnetization behavior of the particles frozen in the matrix to that of the corresponding ferrofluid solution. The previous calculations of Raikher,[7] which describe the anisotropic magnetization process due to the texture induced by the preparation magnetic field, have been extended with success for an assembly of polydisperse superparamagnetic particles and quantitatively compared to our experimental data.

The present results will be useful for understanding magnetic properties of other magnetically textured superparamagnetic systems. They will also help to analyze the optical

anisotropy, arising from the anisotropy of particle orientations, and its influence on the magneto-optical properties of these systems, both from theoretical and experimental points of view.

[1] R. F. Ziolo, E. P. Giannelis, B. A. Weinstein, M. P. O'Horo, B. N. Ganguly, V. Mehrotra, M. W. Russell, and D. R. Huffman, Science **257**, 219 (1992).

[2] J. K. Vassiliou, V. Mehrotra, M. W. Russell, E. P. Giannelis, R. D. McMichael, R. D. Shull, and R. F. Ziolo, J. Appl. Phys. **73**, 5109 (1993).

[3] F. Chaput, J.-P. Boilot, M. Canva, A. Brun, R. Perzynski, and D. Zins, J. Non-Cryst. Solids **160**, 177 (1993).

[4] D. Niznansky, J. L. Rehspringer, and M. Drillon, IEEE Trans. Magn. **30**, 821 (1994).

[5] O. Jarjayes, P. H. Fries, and G. Bidan, J. Magn. Magn. Mater. **137**, 205 (1994).

[6] J. L. Dormann, F. D'Orazio, F. Lucari, E. Tronc, P. Prené, J. P. Jolivet, D. Fiorani, R. Cherkaoui, and M. Noguès, Phys. Rev. B **53**, 14291 (1996) and references therein.

[7] Yu. L. Raikher, J. Magn. Magn. Mater. **39**, 11 (1983).

[8] R. W. Chantrell, N. Y. Ayoub, and J. Popplewell, J. Magn. Magn. Mater. **53**, 199 (1985).

[9] M. I. Shliomis and Yu. L. Raikher, IEEE Trans. Magn. **16**, 237 (1980).

[10] I. Yasumori, D. Reinen, and P. W. Selwood, J. Appl. Phys. **34**, 3544 (1963).

[11] L. Liébert, A. Martinet, and L. Strzelecki, J. Colloid Interface Sci. **41**, 391 (1972).

[12] D. Chandesris, A. Martinet, and L. Strzelecki, Rev. Phys. Appl. **12**, 873 (1977).

[13] L. Néel, C. R. Acad. Bulg. Sci. **228**, 664 (1949).

[14] C. P. Bean and J. D. Livingston, J. Appl. Phys. **30**, 120S (1959).

[15] J.-C. Bacri, R. Perzynski, D. Salin, V. Cabuil, and R. Massart, J. Magn. Magn. Mater. **62**, 36 (1986).

[16] M. Canva, G. Le Saux, P. Georges, A. Brun, F. Chaput, and J.-P. Boilot, Opt. Lett. **17**, 218 (1992).

[17] R. Kaiser and G. Miskolczy, J. Appl. Phys. **41**, 1064 (1970).

[18] C. J. Brinker and G. W. Scherer, *Sol-gel Science: The Physics and Chemistry of Sol-gel Processing* (Academic, Boston, MA, 1990).

[19] *Sol-Gel Optics I, II, III*, Proceedings of SPIE, edited by J. D. Mackenzie, San Diego, CA (International Society for Optical Engineering, Bellingham, WA, 1990, 1992, 1994), Vol. 1328, Vol. 1758, Vol. 2288.

[20] M. Faloss, M. Canva, P. Georges, A. Brun, F. Chaput, and J.-P. Boilot, Appl. Opt. **36**, 27 (1997).

[21] J. Biteau, F. Chaput, and J.-P. Boilot, J. Phys. Chem. **100**, 9024 (1996).

[22] B. Darracq, M. Canva, F. Chaput, J.-P. Boilot, D. Riehl, Y. Lévy, and A. Brun, Appl. Phys. Lett. **70**, 292 (1997).

[23] D. Riehl, F. Chaput, Y. Lévy, J.-P. Boilot, F. Kajzar, and P.-A. Chollet, Chem. Phys. Lett. **245**, 36 (1995).

[24] F. Bentivegna, M. Canva, A. Brun, F. Chaput, and J.-P. Boilot, J. Appl. Phys. **80**, 4655 (1996).

[25] R. Massard, IEEE Trans. Magn. **17**, 1247 (1981).

[26] C. Colliex, J. Electron Microsc. **45**, 44 (1996).

[27] C. Colliex, M. Tencé, E. Lefèvre, C. Mory, H. Gu, D. Bouchet, and C. Jeanguillaume, Mikrochim. Acta **114/115**, 71 (1994).

[28] H. L. Frazer, I. P. Jones, and M. H. Loretto, Philos. Mag. **35**, 159 (1977).

[29] G. Cliff and G. W. Lorimer, J. Microsc. **103**, 203 (1975).

[30] R. D. Leapman, *Transmission Electron Energy-loss Spectrometry in Materials Science*, edited by M. M. Disko, C. C. Ahn and B. Fultz (TMS, Warrendale, 1992), p. 47.

[31] *Proceedings of the 5th International Congress X-rays Optics and Microanalysis*, edited by R. Tixier, J. Philibert, G. Möllenstedt, and H. Gankler (Springer, Berlin, 1969), p. 180.

[32] R. F. Egerton, *Electron Energy-loss in the Electron Microscope* (Plenum, New York, 1986), p. 159.

[33] D. Imhoff, N. Mozdzierz, and M. Backhaus-Ricoult, Microsc. Microanal. Microstruct. **6**, 205 (1995).

[34] C. Colliex, T. Manoubi, and C. Ortiz, Phys. Rev. B **44**, 11402 (1991).

[35] J. L. Dormann, Rev. Phys. Appl. **16**, 275 (1981).

[36] P. J. Flanders, J. Appl. Phys. **63**, 3940 (1988).

[37] H. W. Davies and J. P. Llewellyn, J. Phys. D **12**, 1357 (1979).

[38] J. Ferré and G. Gehring, Rep. Prog. Phys. **47**, 513 (1984).

[39] P. V. Hendriksen, F. Bødker, S. Linderoth, S. Wells, and S. Mørup, J. Phys.: Condens. Matter **6**, 3081 (1994).

[40] R. Sappey, E. Vincent, N. Hadacek, F. Chaput, J.-P. Boilot, and D. Zins, Phys. Rev. B **56**, 14 551 (1997).